Numerical Fracture mechanics based prediction for the roughening of brittle cracks in 2D disordered solids

Lamine Konate, Djimédo Kondo, Laurent Ponson

International Journal of Fracture manuscript No.
(will be inserted by the editor)

Numerical Fracture mechanics based prediction for the roughening of brittle cracks in 2D disordered solids

Lamine Konate · Djimédo Kondo · Laurent Ponson*

Received: date / Accepted: date

Abstract The behavior of fractures in 2D brittle disordered materials results from the competition between the microstructural disorder that roughens cracks and the material elasticity that straightens them. The experimental fracture surfaces left behind are generally scale invariant and their complex geometry are still largely unexplained. Here, this issue is addressed numerically using the boundary element method that predicts incrementally the trajectory followed by cracks in an infinite elastic medium with a heterogeneous field of fracture energy. The predicted fracture surfaces are characterized using their height-height correlation functions and show scale invariant properties. In particular, simulated cracks are shown to follow a random walk with roughness exponent $\zeta = 0.5$, irrespective of the level of microstructural disorder, indicating that the crack behavior is neither persistent nor anti-persistent, but instead, that the orientation of the next propagation increment is chosen randomly, independently of the past trajectory. This behavior is then interpreted from fracture mechanics calculations that show that the restoring force emerging from elasticity that generally straightens cracks vanishes in the limit of large specimens with respect to the characteristic size of the material heterogeneity. This result sheds light on some experimental fracture patterns recently reported and suggests an explanation for the observation of two different types of fracture morphologies in 2D disordered brittle solids.

Institut Jean le Rond d'Alembert (UMR 7190), CNRS - Sorbonne Université, 75005 Paris, France
e-mail: laurent.ponson@upmc.fr

1 Introduction

The study of the morphology of fracture surfaces is a valuable tool for exploring the elementary failure mechanisms involved in heterogeneous materials, since it reflects the interaction of a crack with the material microstructure. Over the last three decades since the pioneering work of Mandelbrot et al. (1984), new fractographic approaches based on the *statistical* analysis of the topography of fracture surfaces have emerged. They have brought out the remarkable scale invariant properties of the roughness of cracks that can be described by scaling exponents that are, to a large extent, independent of the material investigated (see Bonamy and Bouchaud (2011) for a review). These puzzling findings have motivated the development of models of crack growth in disordered solids to explain the universal scaling properties of fracture surfaces (see Alava et al. (2006) for a review). It ultimately led to the development of new approaches in Fracture Mechanics that aim at taking into account the role of the microstructural disorder on the failure of materials, beyond the morphology of fracture surfaces, and in particular the crack growth resistance and its relationship with the microstructural features of materials (Patinet et al. (2013); Demery et al. (2014); Lebihain (2019)). Overall, the statistical investigation of fracture surfaces has provided new and rich insights on the elementary mechanisms of crack growth (see Ponson (2016) for a review). On top of it, it gave birth to a new engineering technique, referred to as statistical fractography, that permits the measurement of the toughness of materials from the statistical analysis of their fracture surfaces (Vernède et al. (2015); Srivastava et al.

(2014); Osovski et al. (2015); Vernède and Ponson (2015); Barak et al. (2019); Auvray et al. (2019)).

The roughness of fracture surfaces exhibit self-affine properties: Crack profiles remain statistically invariant by the transformation $h(\lambda x) = \lambda^{\zeta} h(x)$ where $h(x)$ is the height of the surface, x is the coordinate along an axis parallel to the mean fracture plane and λ is a scaling factor. The exponent ζ is a parameter known as the Hurst or *roughness exponent*. Its value provides the persistency of the cracking process, a property that emerges from the *sign* of the geometrical perturbations along the crack path and its correlations: If $\zeta > 1/2$, the perturbations of the crack path with respect to the straight trajectory is more likely to be upward (resp. downward) if the current propagation direction is also upward (resp. downward). The crack trajectory is then said to be persistent, as the crack tends to propagate along the same direction. On the contrary, for an anti-persistent crack path for which $\zeta < 1/2$, the sign of the propagation direction is more likely to change. A limit case between both behaviors is the random walk characterized by $\zeta = 1/2$ for which the probability to propagate upward and downward are the same, irrespective of the past trajectory. Note that the random walk is the only case that does not lead to spatial correlations of the sign of the perturbations along the crack path.

Fracture experiments performed on 3D materials lead to two-dimensional fracture surfaces. The roughness can then be analyzed either along the crack front direction or along the crack propagation direction. To study the persistency of the crack trajectory, it is then natural to investigate the propagation direction. It has been shown that the scaling behavior of the fracture surface was depending on the *scale* of observation (Bonamy et al. (2006); Vernède et al. (2015)): Beyond a material dependent length scale ξ that provides the characteristic size of the damage and dissipative processes taking place at the crack tip vicinity, the roughness displays an anti-persistent behavior. For example, Millman et al. (1994) found a Hurst exponent $\zeta \simeq 0.4$ in tungsten and in graphite. Boffa et al. (1998) reported an exponent close to $\zeta \simeq 0.45$ in sandstone. Ponson et al. (2006a) and Cambonie et al. (2015) investigated the self-affine properties of fractured sintered ceramics with various combinations of porosity and grain size and reported exponents in the range $\zeta \simeq 0.3 - 0.5$. Last but not least, Dalmas et al. (2008) reported a logarithmic roughness, reminiscent of a vanishingly small roughness exponent $\zeta = 0$, in phase-separated glasses. When investigated at scales much larger than the dissipative processes localized near the crack tip, all solids are brittle. The roughness of fracture surfaces is then signature of the out-of-plane excursions of the crack front that gets around the toughest material regions (Ramanathan et al. (1997); Bonamy et al. (2006); Ponson (2007); Lebihain et al. (2020)). The trajectory of brittle cracks are then *anti-persistent*, as the crack tends to come back within the mean fracture plane after any geometrical perturbations resulting from material inhomogeneities.

At small scales, *i.e.* within the process zone, crack growth proceeds through damage coalescence so that the crack path is controlled by the process of nucleation, growth and coalescence of microcracks or cavities. At these scales, the scaling properties of the fracture roughness are then fundamentally different from those of brittle cracks. In particular, the roughness exponent is reported in the range $\zeta \simeq 0.6 - 0.8$ for a wide range of materials, like metallic alloys, mortar, ceramics, rocks...(Bouchaud et al. (1990); Måløy et al. (1992); Ponson et al. (2006b); Bonamy et al. (2006); Morel et al. (2008)), as long as these fracture surfaces are investigated at scales smaller than the characteristic size of the damage accompanying crack growth. Such a persistent behavior is reminiscent of the elementary process of crack growth at these small scales: Microcrack nucleation is likely to take place in a region located ahead the current crack propagation direction, as the tensile stress is larger along this particular direction. As a result, microcracks tend to align along the current crack orientation. Owing to the attraction exerted by two neighboring cracks (Schwaab et al. (2018)), they end up coalescing together, letting behind fracture surfaces with persistent fracture patterns. Various theoretical models have been proposed to take into account the key role of damage in the process of roughening in 3D solids, like for e.g. the one proposed by Hansen and Schmittbuhl (2003). While they describe the persistent behavior of fracture surfaces, they do not fully capture the complexity of the morphology of fracture surfaces as observed experimentally at small scales (Vernède et al. (2015)). Overall, fracture surfaces resulting from the failure of 3D solids observed over a sufficiently large range of length scales show two different scaling behaviors: At small scales $\delta x \ll \xi$ where ξ is the characteristic size of the damage coalescence process, the crack follows a persistent trajectory with $\zeta \simeq 0.6 - 0.8$ while at large scale $\delta x \gg \xi$, the crack path is anti-persistent displaying either self-

affine properties with an exponent $\zeta \simeq 0.4$ or logarithmic correlations of heights. And each behavior emerges from the two main elementary mechanisms of crack growth, i.e. damage coalescence vs brittle crack growth.

When cracks propagate in very thin specimens, *i.e.* with a thickness comparable to the size of the characteristic microstructural feature of the material, fracture gives rise to a one-dimensional crack profile for which the value of the roughness exponent is *a priori* different than for 3D materials. Indeed, failure consists of the propagation of a crack tip in a 2D plane, a geometry that fundamentally differs from the motion of a crack front in a 3D material. In 2D, experimental studies have been largely devoted to paper sheets. Roughness exponent in the range $\zeta \simeq 0.6 - 0.7$ have been reported by Kertesz et al. (1993); Salminen et al. (2003); Mallick et al. (2007); Bouchbinder et al. (2006). This behavior is also reported in 3D materials like wood by (Engøy et al. (1994)) or in highly textured metallic alloys by (Morel et al. (2004)). But there, the material microstructure is essentially invariant in one direction so that it gives rise to the failure of an effective 2D solid. These experimentally measured scaling properties are well captured by models of crack growth in 2D media where propagation takes place through the coalescence of one or several cavities (Hansen et al. (1991); Zapperi et al. (2005); Bouchbinder et al. (2004); Ben-Dayan et al. (2006)). This suggests that in thin sheets too, persistent crack trajectories with $\zeta > 0.5$ are signature of damage coalescence.

By analogy with the roughening scenario in 3D solids, it is tempting to conjecture that brittle failure in thin specimens might result in anti-persistent ($\zeta < 0.5$) crack trajectories. However, no experimental evidence supports this prediction. On the contrary, recent theoretical investigations of crack growth in 2D disordered brittle solids question the relevance of self-affine concepts to describe crack paths (Katzav et al. (2007); Katzav and Adda-Bedia (2013)). Their predictions derived from linear elastic fracture mechanics even suggest that crack propagation could lead to an apparent roughness exponent larger than one half, even for perfectly brittle solids.

Here, we investigate numerically the roughening of cracks in 2D disordered brittle solids using an original approach. We adapt the Displacement Discontinuity Method (DDM), a boundary element method developed originally for homogeneous elastic media (Crouch and Starfield (1983)), to describe crack growth in materials displaying spatial variations of fracture toughness. With this approach, one can then compute crack paths in elastic media with random failure properties over a wide range of length scales, as the DDM techniques requires the mesh of the free surfaces of the crack only. The main result of our simulations is that, in the limit of large specimens, a self-affine description of the roughness of cracks is appropriate and that crack paths in brittle materials with disorder distribution of fracture properties follow a *random walk* with an exponent $\zeta = 1/2$. Our numerical experiments complete the roughening scenario in 2D solids by evidencing a second class of roughness, different from the persistent fracture profiles with an exponent $\zeta \simeq 0.6 - 07$ reported so far. The transition between both roughening regimes is discussed and compared with the transition observed in 3D solids that also gives rise to two different roughening regimes.

The article is organized as follows: Section 2 recalls the basic principles of the DDM. Section 3 extends the applicability of this technique to disordered materials. The numerical implementation of the method is provided in Section 4. The statistical properties of the computed crack paths are then determined in Section 5. Finally, our results and their implications on the roughening mechanism in 2D disordered materials are discussed in Section 6.

2 Basic principles of the displacement discontinuity method

The numerical approach used for this study is the Displacement Discontinuity Method (DDM) which belongs to boundary elements methods. It has been initially developed by Crouch and Starfield (1983) and presents an enormous advantage for the simulation of crack propagation in elastic media with respect to classical methods like finite elements or even other boundary elements methods: elasticity problems with complex geometry can be solved by meshing only the domain boundary and discontinuities. Moreover, for large specimens that will be considered here, there is no need to mesh the domain boundary. As a result, brittle crack propagation does not require remeshing, but calls for additional nodes along the new crack segments. This allows for the investigation of crack propagation over long distance, up to five orders of magnitude larger than the mesh size, relevant to investigate scaling geometrical properties of the crack roughness. This method has been developed in the context of homogeneous elastic solids and has been ap-

plied to a wide range of fracture problems including cracks interaction (Silva and Einstein (2013); Schwaab et al. (2018)), mixed-mode failure (Meng et al. (2013)) or interfacial fracture (Ortiz and Cisilino (2005)), to quote a few. We remind below the scientific background of the approach and illustrate the methodology through a few simples examples.

2.1 Basic concepts of the method

The displacement discontinuity method is based on the analytic resolution of the problem of a constant displacement discontinuity over a finite line segment in the x, y plane of an infinite elastic solid. The line segment may be chosen to occupy a certain portion of the x-axis, say the portion $|x| \leq a, y = 0$ (see Fig. 1). If we consider this segment to be a line crack, we can distinguish its two surfaces by saying that one surface is on the positive side of $y = 0$, denoted $y = 0_+$, and the other is on the negative side, denoted $y = 0_-$. In crossing from one side to the other, the displacements undergo a constant specified change in value $D_i = (D_x, D_y)$.

We will define the displacement discontinuity D_i as the difference in displacement between the two sides of the segment as follows:

$$
\begin{aligned}
D_i &= u_i(x_1, 0_-) - u_i(x_1, 0_+) \\
D_x &= u_x(x, 0_-) - u_x(x, 0_+) \\
D_y &= u_y(x, 0_-) - u_y(x, 0_+)
\end{aligned}
$$

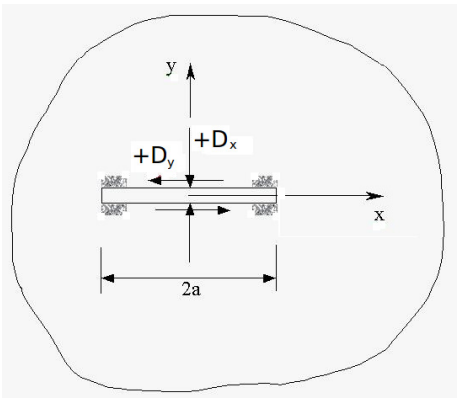

Fig. 1 Components of the discontinuity D_x and D_y.

The solution of this problem is given by Crouch (1976), based on the use of Neuber-Papkovitch potentials.

2.2 Generalization to complex crack paths

In this section, we briefly describe how to implement the DDM for general problems with complex crack geometries. This numerical procedure is depicted in Fig. 2. In this case, the crack is curved,

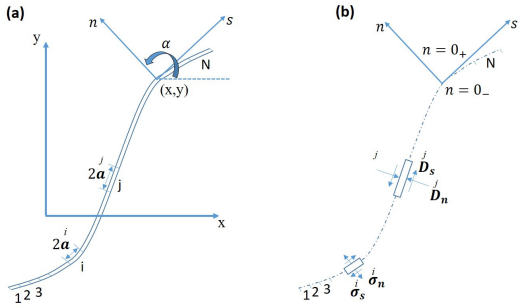

Fig. 2 Representation of a curved crack in an infinite medium by N elements.

but it is discretized with sufficient accuracy by N straight lines joined end to end. The tangential and normal components of displacement discontinuities vector, assumed constant on each segment, are defined with respect to the local coordinates s and n as indicated on the figure:

$$
\begin{aligned}
\overset{j}{D}_s &= \overset{j}{u}_s^- - \overset{j}{u}_s^+ \\
\overset{j}{D}_n &= \overset{j}{u}_n^- - \overset{j}{u}_n^+
\end{aligned}
$$

Thus, the effects of a single elementary displacement discontinuity on the displacements and stresses field in the infinite solid can then be computed provided a suitable transformation of the equations to account for the position and orientation of the line segment in question is done. In particular, the shear and normal stresses at the midpoint of the i^{th} element in figure can be expressed in terms of the displacement discontinuity components at the j^{th} element as follows:

$$
\left.
\begin{aligned}
\overset{i}{\sigma}_s &= \overset{ij}{A}_{ss} \overset{j}{D}_s + \overset{ij}{A}_{sn} \overset{j}{D}_n \\
\overset{i}{\sigma}_n &= \overset{ij}{A}_{ns} \overset{j}{D}_s + \overset{ij}{A}_{nn} \overset{j}{D}_n
\end{aligned}
\right\} \qquad i = 1, N \qquad (1)
$$

where $\overset{ij}{A}_{ss}$, etc.., are the influence coefficients for the stresses. The coefficient $\overset{ij}{A}_{ns}$, for example, gives the contribution to the normal stress at the midpoint of the i^{th} element (i.e. $\overset{i}{\sigma}_n$) due to a constant unit shear displacement discontinuity over the j^{th} element.

By superposition, the stresses $\overset{i}{\sigma}_s$ and $\overset{i}{\sigma}_n$ at the i^{th} element induced by the displacements discontinuities of the N elements can be deduced as

$$\left.\begin{aligned}\overset{i}{\sigma}_s &= \sum_{j=1}^{N} \overset{ij}{A}_{ss}\overset{j}{D}_s + \sum_{j=1}^{N} \overset{ij}{A}_{sn}\overset{j}{D}_n - \sigma_s^{\text{ext}} \\ \overset{i}{\sigma}_n &= \sum_{j=1}^{N} \overset{ij}{A}_{ns}\overset{j}{D}_s + \sum_{j=1}^{N} \overset{ij}{A}_{nn}\overset{j}{D}_n - \sigma_n^{\text{ext}}\end{aligned}\right\} \quad i = 1, N \tag{2}$$

The values of the stresses $\overset{i}{\sigma}_s$ and $\overset{i}{\sigma}_n$ being specified by the boundary conditions for each element of the crack, Eqs. (2) provide a system of $2N$ linear equations with $2N$ unknowns, namely the displacement discontinuities $\overset{i}{D}_s$ and $\overset{i}{D}_n$ for $i = 1$ to N. Since only free surfaces are considered here, these boundary conditions on the crack read as $\overset{i}{\sigma}_s = \overset{i}{\sigma}_n = 0 \,\forall\, i$. The values of the σ_s^{ext} and σ_n^{ext} are prescribed by the imposed stress conditions at infinity, in shear and tension, respectively.

This linear system of equations can be solved for $\overset{j}{D}_y$, $j = 1$ to N, by standard numerical methods. Again, from the knowledge of the $\overset{j}{D}_y$'s, one can calculate the stress and displacement field in the whole system by summing the contributions of each element (see Crouch and Starfield (1983)). One can also compute the elastic energy release rate at the tip of the crack, as detailed in Sec. 3.1.

3 Extension to the propagation of cracks in heterogeneous media

We adapt now the DDM method to investigate crack propagation, notably in materials with heterogeneous fracture properties.

3.1 Criterion on the propagation direction

To predict the crack trajectory, we first need a criterion on the propagation direction. Classically, crack path criteria can be chosen among the principle of local symmetry proposed by Cotterell and Rice (1980) and Gol'dstein and Salganik (1974), the maximum tangential stress criterion proposed by Erdogan and Sih (1963) and the maximum strain energy release rate proposed by Hussain et al. (1974). We use here the maximum strain energy release rate criterion, as it can be naturally extended to heterogeneous materials, as done by Chambolle et al. (2009) and Hakim and Karma (2009). In homogeneous media, it predicts that crack propagates along the direction θ_c which *maximizes* the elastic energy release rate, *i.e.* $G(\theta_c) = \underset{\theta}{\text{Max}}[G(\theta)]$. Following Shen and Stephansson (1994), we implement this criterion by computing $G(\theta)$ within the DDM: The strain energy release rate that corresponds the variation of elastic energy of the fracturing body for a crack growth over a unit length is obtained from the computation of the elastic energy for two subsequent crack configurations. The elastic energy, W, in a 2D linear elastic body $\mathcal{S}$ follows

$$W = \frac{1}{2}\int\int_{\mathcal{S}} \sigma_{ij}\epsilon_{ij} dV$$

where σ_{ij} and ϵ_{ij} are the stress and strain tensors, and V is the volume of the body. As a result, the elastic energy can also be calculated from the stresses and displacements along its boundary $\mathcal{C}$ using Green's theorem

$$W = \frac{1}{2}\int_c \sigma_s u_s + \sigma_n u_n ds.$$

Applying this equation in the case of an infinity body with far-field stresses σ_s^{ext} and σ_n^{ext}, the strain energy, W, reads

$$W = \frac{1}{2}\int_0^a (\sigma_s - \sigma_s^{\text{ext}}) + (\sigma_n - \sigma_n^{\text{ext}}) u_n ds. \tag{3}$$

Owing the displacement discontinuity on the crack face, this expression leads to:

$$W \approx \frac{1}{2}\sum_i (a^i(\sigma_s^i - \sigma_s^{\text{ext}})D_s^i + a^i(\sigma_n^i - \sigma_n^{\text{ext}})D_n^i) \tag{4}$$

That sum can be calculated from the D^i's determined by the DDM. Where $\{\sigma_s^i = 0,\, \sigma_n^i = 0\}$ are given by the boundary conditions on the crack surfaces and $\{\sigma_{\text{n}}^{\text{ext}} = \sigma_\infty,\, \sigma_{\text{s}}^{\text{ext}} = 0\}$ corresponds to pure tensile loading conditions considered in the following. The elastic energy release rate can then be estimated from

$$G(\theta) = -\frac{\partial W}{\partial a} \approx \frac{[W(a) - W(a + \Delta a)]}{\Delta a}$$

where $W(a)$ is the elastic energy corresponding to the original crack configuration, while $W(a + \Delta a)$ is the elastic energy of the original crack, a, extended by Δa along the direction θ as illustrated in Fig. 3. The elastic energy rate is then evaluated in the range $[-45° \leq \theta \leq 45°]$ by step of one degree to identify the propagation direction θ_c that maximizes $G(\theta)$.

	θ_c	$G(\theta_c)$
DDM (This study)	$-54°$	$388\,\mathrm{J.m^{-2}}$
DDM (Shen and Stephansson (1994))	$-55°$	$390\,\mathrm{J.m^{-2}}$
Maximum tensile stress criterion (Hussain et al. (1974))	$-57°$	$390\,\mathrm{J.m^{-2}}$
Melin's results, crack kink (Melin (1985))	$-55°$	$384\,\mathrm{J.m^{-2}}$

Table 1 Comparison of the kink angle θ_c and the elastic energy release rate $G(\theta_c)$ as obtained from our method with results of the literature for the test case of a crack with inclination $\alpha = 45°$ illustrated in Fig. 4(a).

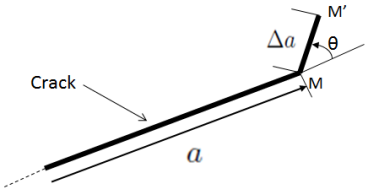

Fig. 3 Extension of the original crack of length a of an elementary increment Δa.

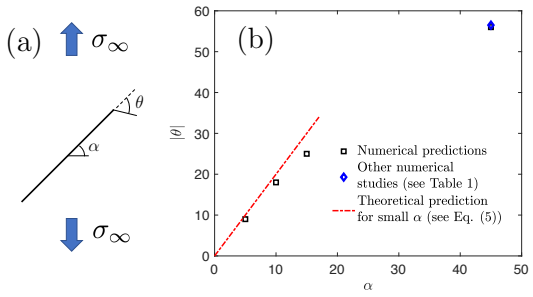

Fig. 4 Validation of the proposed numerical approach on a test case: (a) Inclined crack in an infinite homogeneous medium under traction. The imposed stress is $\sigma_\infty = 10$ MPa while the elastic properties of the material are $E = 6.2$ GPa and $\nu = 0.28$. (b) Comparison of the computed kink angle $|\theta|$ with other numerical results of the literature for $\alpha = 45°$ and with the analytical prediction of Eq. (5) valid in the limit of slightly inclined cracks

3.2 Preliminary validation of the model: Prediction of the kink angle of an inclined tensile crack

To test the numerical procedure described previously, we compare its predictions with available results in the literature on a test case. A homogeneous infinite medium submitted to a tensile stress with a crack of inclination α is considered (see Fig. 4(a)). We are interested by the kink angle θ_c and the corresponding value of the elastic energy release rate $G(\theta_c)$. Table 1 compares the results of our simulations with numerical findings of other studies like the ones of Shen and Stephansson (1994), Hussain et al. (1974) and Melin (1985) for $\alpha = 45°$. The predictions of the boundary element method is then compared in Fig. 4(b) with theoretical predictions derived in the limit of slightly inclined cracks. The propagation direction follows $\theta = -2\,k_{II}/k_I$ where k_I and k_{II} are the local stress intensity factors in mode I and II before the kink, as predicted by Amestoy and Leblond (1992). Using the expressions $k_I = \sigma_{ext}\cos^2\alpha$ and $k_{II} = \sigma_{ext}\cos\alpha\sin\alpha$ of the stress intensity factors at the tip of a slightly inclined tensile crack, one then obtains

$$\theta_c \simeq -2\alpha. \tag{5}$$

Our numerical results are consistent with this prediction for slightly inclined crack (see Fig. 4(b)), confirming the ability of the numerical approach to predict accurately crack propagation direction.

The rate of convergence of our method is provided in Fig. 5 that shows the error on the computed value of the elastic energy release rate $G(\theta_c)$ along the propagation direction θ_c for the strongly inclined crack $\alpha = 45°$ as a function of the element size Δa. The precision of our calculation is inversely proportional to the number of nodes N used to mesh the initial crack, as it evolves as $|G - G^{conv}|/G^{conv} \sim 1/N$.

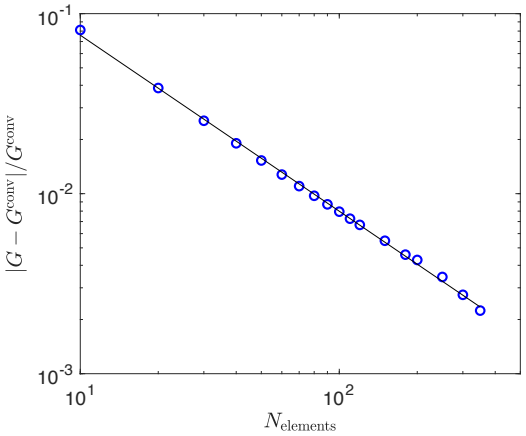

Fig. 5 Convergence rate towards the critical value of the elastic energy release rate $G(\theta_c)^{conv} = 388\,\mathrm{J.m^{-2}}$ along the propagation direction $\theta_c = -54°$ as a function of the number of nodes for the kink problems represented on Fig. 4 for $\alpha = 45°$.

3.3 Modeling of the disordered failure properties

To investigate the effect of microstructural disorder on crack path, we consider a solid with a heterogeneous field of fracture energy $G_c(x,y)$ with the following properties:

- The field of fracture energy is described by a matrix of size $(N_\mathrm{x}+1)\times(N_\mathrm{y}+1)=1001\times 51$ providing the values of G_c at the discrete locations $\{x_\mathrm{i}=i\,d, y_\mathrm{j}=j\,d\}_{-N_\mathrm{x}/2\le i\le N_\mathrm{x}/2,-N_\mathrm{y}/2\le j\le N_\mathrm{y}/2}$ on a regular square network. Each node is separated by a distance ξ along both directions, so that the region of interest is of size $(N_\mathrm{x}\,d, N_\mathrm{y}\,d)$. It turns out that the out-of-plane perturbations of the crack are small enough so that the crack always remain in this domain. The fracture energy for any material point (x,y) is obtained from a linear interpolation from the value of fracture energy of the four nearest nodes.
- d is a material length scale. It provides the spatial extent of the toughness heterogeneities in the material. It can be interpreted as the characteristic size of the dominant microstructural feature, like *e.g.* the grain diameter.
- To model microstructural disorder, the value of G_c at each node is taken from a uniform distribution with average value $\langle G_c\rangle = 1$ and variance $\sigma_{G_c}=\sqrt{<G_c^2>-<G_c>^2}$. σ_{G_c} is a measure of the amplitude of the microstructural disorder in the material.

We now need to extend the criterion of maximum energy release rate adapted to homogeneous media to the case of a material with a heterogeneous distribution of toughness. Following Chambolle et al. (2009) and Hakim and Karma (2009), a crack located initially in M is then expected to propagates until the point M' (see Fig. 4) along the direction θ_c that satisfies

$$\frac{G(\theta_\mathrm{c})}{G_\mathrm{c}(\theta_\mathrm{c})}=\underset{\theta}{\mathrm{Max}}\left[\frac{G(\theta)}{G_\mathrm{c}(\theta)}\right]. \tag{6}$$

Here, $G_\mathrm{c}(\theta)$ is defined as the average fracture energy along the crack path

$$G_c(\theta)=\frac{1}{\Delta a}\int_M^{M'} G_c(s)ds. \tag{7}$$

Δa is the distance between M and M', corresponding to the elementary propagation distance of the crack at each step. In the following, we take $\Delta a \ll \xi$. The linear interpolation of G_c used in our simulations to describe the field of fracture energy at any location results in the simplified expression $G_c(\theta)=\dfrac{G_c(M')+G_c(M)}{2}$.

4 Numerical implementation with adaptative meshing

The numerical method is based on the incremental calculation of the crack evolution. For a given crack configuration, we compute first the elastic energy $W(a)$ stored in the body by solving the system of Eqs. (2) that provides the displacement discontinuities. They are then inserted in the expression of the energy given in Eq. (4). An element is then added at the crack tip along the direction θ as illustrated in Fig 3, and the new energy $W(a+\Delta a)$ is computed, after computing new values of displacements discontinuities. This allows the calculation of the elastic energy released rate $G(\theta)$ along this direction. The procedure is repeated for various directions, in order to determine the variations of the function $G(\theta)$. The maximum energy release criterion of Eq. (6) is then applied and a crack increment along the predicted direction θ_c that maximizes the function $G/G_\mathrm{c}(\theta)$ is added at the crack tip. The procedure is repeated from this new crack configuration, which is the new initial conditions for the next time step. The full numerical procedure is summarized on the flowchart of Fig. 6.

We focus here on the scale invariant properties of the crack path, requiring crack propagation distances several orders of magnitude larger than the characteristic material length scale d. In our simulation, the elementary step Δa of crack growth used in the incremental calculation of the crack evolution is equal to $\Delta a = d/20$. To compute the scaling properties of the crack profiles, we need to achieve propagation over a distance of about $500\,d$. It then requires up to 10^4 time steps during which a system of $2\,N$ linear equations must be solved. Here N is the number of nodes along the crack path that can be as large as 10^4 when a new element is added at each time step. To speed up the computations, the crack path is remeshed during the simulation so that the total number of elements used to describe the crack geometry is limited to a few thousands. Our remeshing strategy is the following: The mesh is separated in two sub-domains. For the part of the crack path close to the crack tip, in a region of length $\simeq 20\,d$, the mesh structure is kept unchanged with a mesh size $\Delta a = d/20$. The mesh in the region far from the tip is changed. The element density is progressively decreased, so that the mesh is less and less refined as we go further away from the crack tip. This approach builds on the theoretical framework of perturbed crack paths in 2D elastic media développed by Cotterell and Rice (1980) who showed that the impact of geometri-

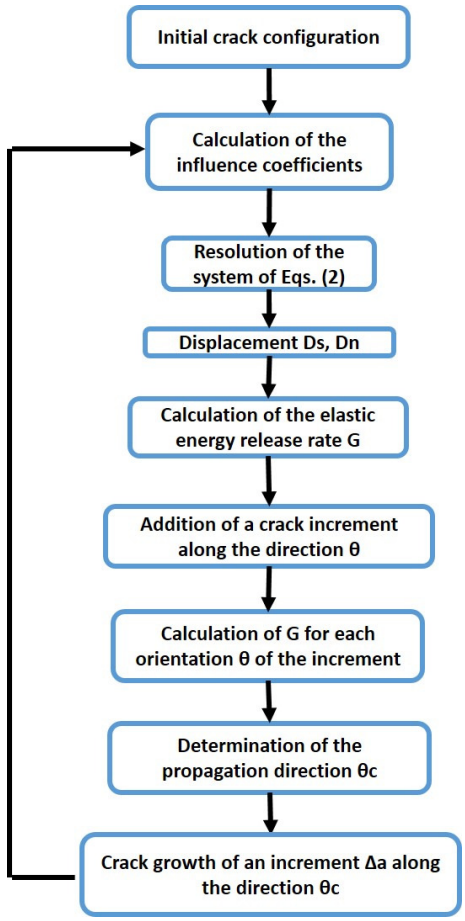

Fig. 6 Flowchart of the numerical scheme used to predict the crack trajectory.

cal perturbations on the value of the stress intensity factors and the resulting elastic energy release rate *decreases* as a power law with the distance to the tip. The differences between crack paths predicted by both approaches are found to be negligible. However, the computational time is drastically reduced with the remeshing methodology. Indeed, with this new procedure, the computational time for each iteration is relatively constant, while it increases exponentially without remeshing since the number of elements increases at each time step. Note also that we did vary the value of the increment size in the range $d/20 \leq \Delta a \leq d/10$ and did not observe any noticeable change in the geometrical properties of the computed crack profiles.

5 Numerical predictions of the scaling properties of crack trajectories in 2D disordered media

In this section, we characterize the geometrical properties of the crack trajectories as computed for an elastic medium with random fracture properties. Crack propagation is investigated in an infinite sample with an initial straight notch of length $a_0 = 20\,d$ located in $|x| \leq 10\,d$. The specimen is submitted to a tensile loading, as shown in Fig. 7(a), with a prescribed imposed value σ_{ext} equals to unity. As we are only interested in the crack geometry, we do not adapt the external loading so that $G = G_c$ at each incremental time step. Instead, we keep the loading constant and at each time step, we impose a crack growth along the direction that maximizes G/G_c.

The sample geometry leads to the propagation of two symmetrical cracks in opposite directions. We impose a constant growth velocity on both sides of the crack, corresponding to an advance by the same incremental length Δa at each iteration of the calculation at both crack tips. Calculations allowing propagation on one side of the crack only give crack trajectories with similar statistical properties, suggesting that both crack tips do no interact with each other. Simulations are run for incremental steps of crack advance much smaller than the heterogeneity size, typically $\Delta a = 0.01 - 0.1\,d$. A typical crack pattern is shown in Fig. 7. Our approach allows for crack propagation over distances larger than $500\,d$ corresponding to tenths of thousand of time steps. The two symmetrical cracks follow different trajectories, but they share common statistical features, since they emerge from the interaction of a tensile crack under similar loading conditions with a heterogeneous material with similar properties. As a result, they can both be used indifferently to investigate the geometrical properties of crack trajectory.

5.1 Numerical results

On a general manner, the interaction of a brittle crack with a disorder microstructure produces scale invariant patterns as long as there is a clear separation between the characteristic heterogeneity size d and any structural length, here the total crack length. To characterize quantitatively these scale invariant properties, it is convenient to compute the correlation function of height variations along the crack trajectory that is defined as

$$\Delta h(\delta x) = \sqrt{\langle (h(x+\delta x) - h(x))^2 \rangle_x} \qquad (8)$$

where $h(x)$ describes the deviations of the crack path from straightness as illustrated in Fig. 7. The function Δh provides the typical height variation between two points separated by the distance δx along the mean crack plane. It also provides the roughness amplitude at a given observation scale

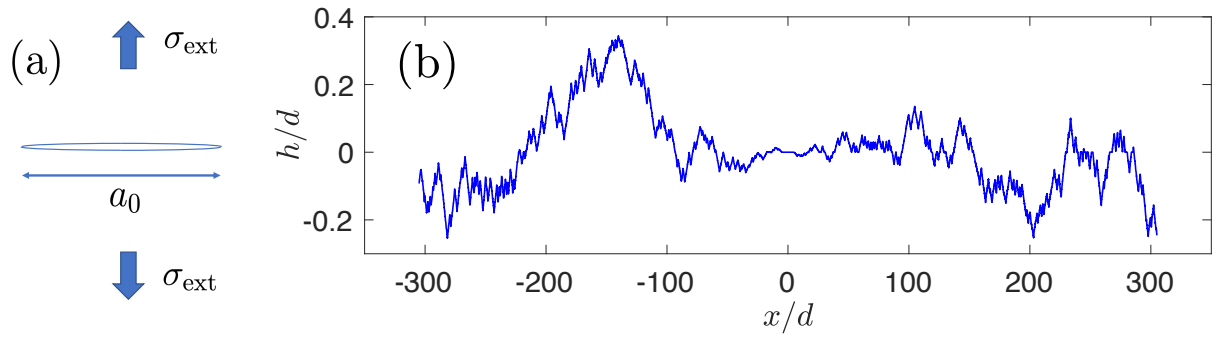

Fig. 7 (a) Geometry of the fracture test used in the calculation. The infinite notched specimen is submitted to pure tensile loading conditions. The crack length priori to initiation is $a_0 = 20\,d$. (b) Typical crack path in a brittle disordered solid obtained by the incremental boundary element method developed in this study.

δx. As a result, the larger δx, the larger the roughness Δh. For a self-affine crack profile, *i.e.* for a trajectory statistically invariant by the transformation $h(x) \rightarrow \lambda^{\zeta} h(\lambda x)$, the correlation function follows the scaling relation

$$\Delta h(\delta x) \sim \delta x^{\zeta} \tag{9}$$

where ζ is the roughness exponent that describes how the roughness Δh varies with the observation scale δx.

The correlation function is computed on the crack profiles obtained by the boundary element method and is shown in Fig. 8 . In order to obtain such smooth variations of the correlation function, Δh is averaged over twelve statistically equivalent crack trajectories corresponding to the same level σ_{G_c} of material disorder, but different realizations of the disorder. For a given simulation, left and right cracks are analyzed separately after the subtraction of the initial straight notch. We could not evidence any transient roughening of the crack profile close to initiation.

The correlation function of Fig. 8 shows two seemingly self-affine regimes, corresponding to both straight lines in this logarithmic representation:

(i) At length scales δx smaller than the heterogeneity size d, the correlation function follows an apparent power law with exponent $\zeta_0 \simeq 0.9$, as shown by the blue straight line shown for $\delta x < d$ in Fig. 8.

(ii) At length scales δx larger than d up to a cut-off length $L_c \simeq 100\,d$, the correlation function also follows a power law, but with a smaller exponent $\zeta \simeq 0.5$ as shown by the red straight line fitting the data for $\delta x > d$. Such a behavior is reminiscent of a *random walk*, *i.e.* a process during which the propagation direction (up or down) is independent of the previous propagation directions. Such a feature is confirmed in the inset of Fig. 8 that provides the correlation function of the local slopes

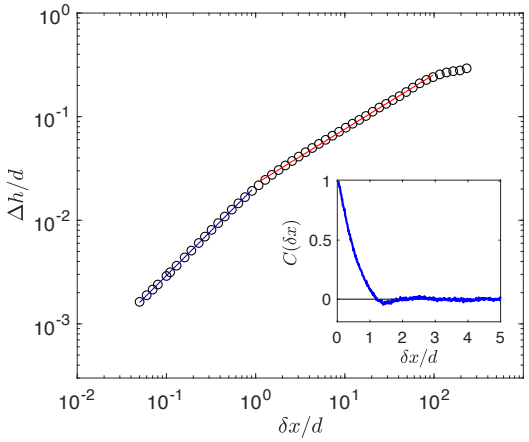

Fig. 8 Height-height correlation function computed for $\sigma_{G_c} = 0.01$, Both axis have been normalized by the heterogeneity size d. The fit of Δh for scales $\delta x < d$ leads to an apparent roughness exponent $\zeta \simeq 0.9$ (blue line) while $\zeta \simeq 0.5$ is obtained at larger scales $\delta x > d$ (red line). The inset shows the correlation function $C(\delta x)$ of the local slopes along the crack path (See Eq. (10)). The slopes are not correlated at large scales $\delta x > d$, as expected for a random walk ($\zeta = 1/2$).

$$C(\delta x) = \left\langle \left.\frac{dh}{dx}\right|_x \left.\frac{dh}{dx}\right|_{x+\delta x} \right\rangle_x . \tag{10}$$

We see here that the slopes along the crack path are effectively not correlated in the regime $\delta x \gg d$, as expected for a random walk. In addition to this property, we explored the scaling behavior of the moments $\Delta h_q(\delta x) = \langle (h(x+\delta x) - h(x))^q \rangle_x^{1/q}$ in the range $0 \leq q \leq 3$, thus extending the investigation of the correlation of height fluctuations beyond the case $q = 2$ shown in Fig. 8. We do observe the same behavior $\Delta h_q(\delta x) \simeq \delta x^{\zeta}$ with $\zeta \simeq 0.50$. This behavior, also referred to as mono-affine, con-

firms that a single exponent $\zeta = 1/2$ is sufficient to describe the self-invariant properties of the fracture profile.

As shown on Fig. 9, the value of these both exponents is actually robust, as it does not depend on the level σ_{G_c} of the microstructural disorder, leading to

$$\begin{cases} \zeta_0 = 0.88 \pm 0.01 & \text{for} \quad \delta x \ll d \\ \zeta \ = 0.51 \pm 0.01 & \text{for} \quad \delta x \gg d. \end{cases} \tag{11}$$

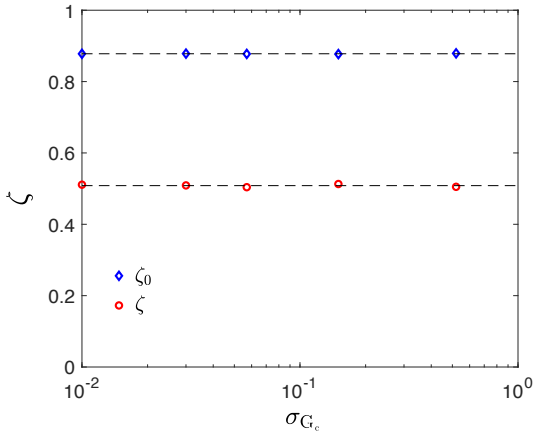

Fig. 9 Variations of the roughness exponents characterizing the scaling behavior of the crack roughness with the amplitude of the material microstructural disorder. ζ_0 is extracted from the power law variations of the correlation function at small scales $\delta x/\xi < 1$ while ζ is extracted from its variations at large scales $\delta x/\xi > 1$. Dotted lines represent the average value with $\zeta_0 = 0.88$ and $\zeta = 0.51$.

The scaling properties of the fracture profile provide insights on the behavior of tensile cracks in disordered materials. Self-affine profiles with roughness exponent $\zeta > 0.5$ indicates a persistent behavior while $\zeta < 0.5$ indicates an anti-persistent behavior: For a positive local slope $dh/dx(x)$ in x, a persistent behavior means a probability larger than $1/2$ to find a positive local slope $dh/dx(x+\delta x) > 0$ at the next elementary step in $x + \delta x$. On the contrary, an anti-persistent behavior means that a negative local slope $dh/dx(x + \delta x) < 0$ is more likely. Here, at scales larger than the heterogeneity size d, the roughness exponent $\zeta \simeq 0.5$ indicates that the crack follows a *random walk*, with no persistency in the sign of the slope dh/dx: The probability for the crack to propagate upward, *i.e.* towards the positive values of h, is equal to the probability to propagate downward, *i.e.* towards the negative values of h, whatever the considered position x along the crack path, and irrespective of the previous propagation directions. At smaller scales $\delta x < a$, the behavior of the crack is clearly different, characterized by an exponent $\zeta \simeq 0.9$ characteristic of a persistent behavior. As shown in the next section, this behavior is reminiscent of the propagation of a crack within a heterogeneity, where the local toughness is slowly varying.

6 Interpretation of the scaling properties of the computed crack profiles

6.1 Interpretation of the small scale scaling regime

Let us first discuss the small scale regime characterized by the seemingly roughness exponent $\zeta_0 \simeq 0.9$. This behavior is observed at scales smaller than the heterogeneity size d, suggesting that it does not emerge from the disordered distribution of fracture energy. Effectively, it is reminiscent of the trajectory of a crack propagating in a monotonously varying toughness field, as at scales $\delta x \ll d$, the fracture energy landscape is determined from a linear interpolation of the toughness between two neighboring heterogeneities (see Sec. 3.3). This suggests that at small scales $\delta x < d$, the crack trajectory is smooth and can be approximated by a straight segment of typical length d. Considering a linear variation $h(x) \sim \delta x$ of height in the expression (9) of the correlation function leads to a linear variation $\Delta h \sim \delta x$ that accounts for the observations made in the small scale regime $\delta x < d$, with an apparent roughness exponent $\zeta_0 \simeq 0.9$. As a result, the power law behavior of the correlation function (with an exponent close to unity) is not reminiscent of scale invariance, a feature that is also observed experimentally when brittle fracture surfaces are investigated at scales smaller than the grain size (see for example Ponson et al. (2006a)).

6.2 Interpretation of the large scale scaling regime

The regime with exponent $\zeta \simeq 1/2$ observed at large scales $\delta x \gg d$ is more interesting. It results from the scale invariant fracture pattern shown in Fig. 7 that displays geometrical perturbations over a broad range of length scales, from $\delta x = L_c \simeq 100\, d$ (see for example the large scale perturbation located in $-200\, d \leq x \leq -100\, d$ in Fig. 7) down to small scale features of size $\delta x \simeq d$. Here, the most interesting property of the computed crack profiles lies in the value of the roughness exponent $\zeta \simeq 0.5$ that is signature of a pure random process, i.e. a propagation direction at each time independent of the past trajectory. This is at odd with the experimental observations made in 2D specimens like for example sheets of papers (Kertesz

et al. (1993); Salminen et al. (2003); Mallick et al. (2007); Bouchbinder et al. (2006)) that report roughness exponents in the range $\zeta \simeq 0.6 - 0.7$ reminiscent of a persistent behavior. It should be emphasized that elasticity does lead to long-range interactions between different regions of a crack (see for example Cotterell and Rice (1980)) so that a pure random behavior is a priori unexpected, even though the distribution of toughness in the medium is purely random.

To explain such a counter-intuitive behavior, we derive the path equation of a crack in a 2D linear elastic medium with randomly distributed fracture properties. The detailed calculation is provided in Ponson et al. (2021). It takes inspiration from the work of Katzav et al. (2007), but considers only variations in *fracture energy*, excluding *elastic* heterogeneities. The final path equation reads

$$\frac{dh}{dx} = -\frac{1}{\sqrt{\mathcal{L}_1}} \int_0^x \frac{\frac{dh}{dx}|_u}{\sqrt{x-u}} du - \frac{h(x)}{\mathcal{L}_2} + \eta(x) \qquad (12)$$

where $\eta(x)$ is a stochastic noise of average value $\langle \eta \rangle_x = 0$ that describes the out-of-plane perturbations resulting from the presence of toughness heterogeneities and $\mathcal{L}_1$ and $\mathcal{L}_1$ are structural lengths emerging from the geometry of the specimen and the applied loading conditions. They can be expressed as the ratio of the amplitude of the second and third order terms in the Williams (1952)' expansion of the stress field near the crack tip (like *e.g.* the T-stress) over the macroscopically applied stress intensity factor $K_{\rm I} = \sigma_\infty \sqrt{\pi a/2}$ (see Ponson et al. (2021) for details). For the geometry considered here in Fig. 7, both lengths are of the order of the total crack length a as there is no other structural length scale in the problem.

In absence of material disorder, *i.e.* $\eta = 0$, the path equation (12) predicts that any geometrical perturbations rapidly vanish so the crack follows a straight trajectory. In particular, the local term (proportional to $-h(x)$) and the non-local term (also referred as the memory term, as it implies that the crack propagation direction in x depends on the slope $dh/dx(u)$ of the crack profile for $u \leq x$) both contribute to flatten the crack profile and maintain it close to the mean fracture plane. In presence of disorder, the noise η tends to roughen the fracture profile, thus competing with these both terms.

It turns out that in the limit $d \ll a$, these both terms can be neglected (see Ponson et al. (2021) for the rigorous proof), leading to the simplified path equation

$$\frac{dh}{dx} = \eta(x) \qquad (13)$$

that is nothing but the governing equation of a random walk. Indeed, the correlator $C(\delta x)$ of the local slopes defined in Eq. (10) can be computed directly from Eq. (13), leading to $C(\delta x) = \langle \eta(x)\, \eta(x + \delta \mathrm{x}) \rangle_x$. As the quenched noise $\eta(x)$ describes the effect on the local crack propagation direction of the random distribution of toughness of the material, it displays short-range correlations, with a correlation length d given by the heterogeneity size. Consequently, the local slopes along the crack profile do not display any correlations at scales larger than d, defining thus a random walk.

This interpretation is tested in the inset of Fig. 8 that shows the correlations of local slopes along the crack path. Correlations vanish for $\delta x \gg d$, in line with the predictions of Eq. (13). According to this equation, the correlator of the local slopes is a direct measurement of the correlations of $\eta(x)$, a quenched noise with no correlation beyond $\delta x > d$. Interestingly, we notice a slight anti-correlation, $C(\delta x \simeq 3/2\, d) < 0$, a phenomenon that is observed irrespective of the amplitude of the material disorder. This effect may result from the two terms of Eq. (12) that has been neglected in the simplified path equation (13). These terms, that promote anti-persistency, i.e. a downward deviation after the crack has been deviated upward, may not be fully negligible even at the scale $\delta x \simeq d$.

In the case considered here where $\mathcal{L}_1 \gg d$ and $\mathcal{L}_2 \gg d$, the effect of the material elasticity on the crack roughening process is rather marginal. Note however that its contribution dominates over the disorder at large scales δx comparable to the total crack length a, thus setting the cut-off length $L_{\rm c} \simeq 100\, d$ of the self-affine regime that we see in Fig. 8.

6.3 Random walk like crack path in materials reinforced by tough inclusions

Building on the better understanding of the origin of the random walk like fractures obtained in our simulations, we can now propose, as an illustration, an example of *realistic* material microstructure that leads to such a behavior. In Figure 10, one considers the case of a 2D brittle solid of toughness $G_{\rm c}^{\rm mat}$ reinforced by tough circular inclusions of toughness $G_{\rm c}^{\rm inc} > G_{\rm c}^{\rm mat}$ with the following hypothesis:

(i) The matrix and the inclusions share the same elastic properties. Under these conditions, the interaction between the crack and an inclusion is *local* as the crack cannot feel the presence

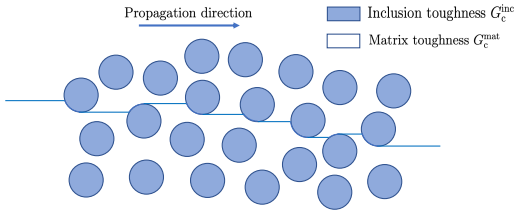

Fig. 10 Crack path in a homogeneously elastic brittle material reinforced by tough circular inclusions. Under the assumptions of large toughness ratio $G_c^{inc}/G_c^{mat} > 3.85$ and scale separation between the inclusion size and the specimen dimension, $d \ll \mathcal{L}$, the crack by-passes each inclusion randomly by the top or by the bottom, letting behind a random walk like fracture profile, in agreement with our numerical predictions.

of the heterogeneities before it lands on the matrix-inclusion interface.

(ii) The toughness ratio between the inclusion and the matrix is larger than the critical ratio $\left(G_c^{inc}/G_c^{mat}\right)_c \simeq 3.85$ beyond which the inclusions are systematically by-passed by the crack. This critical ratio, obtained from the theoretical formulae of Amestoy and Leblond (1992), corresponds to the minimal toughness ratio for which a crack, after landing on the equatorial plane of the circular inclusion, will still kink with an angle $\theta = 90°$ to by-pass the inclusion (Lebihain et al. (2020)). Note that we do not consider here the case where the inclusion-matrix interface has different fracture properties than the inclusion itself.

(iii) The inclusion diameter d is much lower than any structural length scales (*e.g.* any specimen dimension), so that the elastic restoring terms in the path equation (12) can be neglected.

Under these conditions, the crack trajectory within the matrix or within the inclusions is straight, perpendicular to the axis of application of the tensile loading, as represented in Fig. 10. The deviations from straightness arise only from inclusion by-pass. This mechanism has been investigated by Faber and Evans (1983) and then by Lebihain (2019) for different inclusion geometries and properties: The inclusions considered here are by-passed either by the top or by the bottom, the landing height of the crack on the inclusion selecting one or the other mechanism. If the crack lands on the upper half, the inclusion is by-passed by the top while a crack landing on the lower half leads to a bypass by the bottom so that the probability for each mechanism is the same.

The emergence of random walk like fracture profiles is now clear in this example. The crack is deviated along the upper or lower direction with the same probability, irrespective of the previous crack trajectory, as expected for a random walk. It should be emphasized that the out-of-plane deviations of the crack emerge here from the *discontinuities* in the toughness field at the matrix-inclusion interface. This type of modeling based on a realistic description of the material microstructure captures the properties of scale invariance of the fracture profile, but also the *amplitude* of the roughness, that can be related to the size and density of inclusions (see for example Lebihain et al. (2020)). Our approach, despite its ability to predict the scale invariant properties of crack profiles, is not adapted to investigate the effect of microstructural parameters on the amplitude of the crack out-of-plane deviations as the roughness amplitude does not converge to a finite value in the limit $\Delta a \to 0$.[1]

7 Conclusion and comparison with experimental observations

The scale invariant properties of cracks in 2D elastic materials with disordered fracture properties have been investigated by the DDM method that allows for the fast calculation of crack profiles over sufficiently long distances. Our numerical observations suggest that cracks follow random walks ($\zeta = 1/2$), as long as fracture profiles are observed at scales larger than the characteristic heterogeneity size and smaller than any structural length scale. This result represents a reference case for comparison with experiments.

How, then, can one reconcile our numerical predictions (supported by theoretical arguments) with the experimental investigations of crack roughening in 2D disordered materials that report persistent crack profiles with roughness exponents in the range $\zeta = 0.6 - 0.7$? Our fracture mechanics based method assumes that all the dissipative mechanisms that take place at the crack tip vicinity during propagation are confined in a zone of size ℓ_{pz} *smaller* than the incremental propagation distance Δa, and, as a consequence, *smaller* than the heterogeneity size $d \gg \Delta a$. This assumption is in contradiction with most experimental situations investigated so far. For example, in paper sheets that have been largely used in experiments, damage may be observed at the millimeter scale ahead

[1] The development of $G(\theta)/G_c(\theta) \simeq 1 - \cos^2(\theta) + \Delta a/d\, f(\theta)$ around small angles $\theta \ll 1$ for a *continuous* variation of G_c shows that the limit $\Delta a/d \to 0$ corresponds to a straight path as the crack propagation direction along which this ratio is maximal converges then to $\theta_{max} \to 0$.

of the crack tip, leading to $\ell_{\rm pz} \simeq 1$ mm while the heterogeneities are of the order of the fiber size, *i.e.* $d \simeq 100\,\mu$m, suggesting that crack trajectory is controlled by the process of damage coalescence in paper sheet.

This observation, together with our numerical work, suggests a unified scenario for crack paths in thin sheets:

(i) When the assumption of *brittle* failure of disordered material is enforced, namely $\ell_{\rm pz} \ll d$ where d is the size of the characteristic microstructural features, one may expect a *random walk* behavior with $\zeta = 1/2$, under the conditions that crack profiles are investigated in the range $d < \delta x < \mathcal{L}$;

(ii) when the fracture process zone is larger than the heterogeneity size, $\ell_{\rm pz} > d$, crack path is controlled by damage coalescence as shown by Hansen et al. (1991), Zapperi et al. (2005), Bouchbinder et al. (2004) and Ben-Dayan et al. (2006). We then expect *persistent* fracture profiles with roughness exponent $\zeta \simeq 0.6 - 0.7$.

In addition to this difference in the value of the roughness exponent, we may notice that brittle failure leads to mono-affine fracture profiles, like in the present study, while damage coalescence leads to multi-affine scaling properties, in line with the observations made on fracture surfaces of 3D solids by Vernède et al. (2015).

This proposed scenario is supported by the experimental study of Ramos et al. (2013) where large heterogeneities, in the millimeter range, were inserted artificially in a sheet of paper. By upscaling the heterogeneity size above the characteristic size of the damage processes, the crack path was shown to crossover from a persistent behavior to a random walk like geometry with roughness exponent $\zeta \simeq 0.49 \pm 0.03$. A very recent study by Ponson et al. (2021) combining an experimental and numerical investigation of crack profiles in 2D consolidated granular solids comes also to support this scenario. We believe that these ideas could be further tested and consolidated by investigating fracture profiles in architectured materials with tunable microstructures where the ratio $\ell_{\rm pz}/d$ can be continuously varied, using for example 3D printed techniques in the spirit of recent works of Wang and Xia (2017) and Albertini et al. (2020).

The authors would like to thank their colleague and friend Jean-Baptiste Leblond for the uncountable and insightful discussions about the modeling of crack growth in heterogeneous solids, and more generally, for his contagious enthusiasm and endless curiosity.

References

Alava, M.J., Nukala, P.K., Zapperi, S., 2006. Statistical models of fracture. Adv. Phys. 55, 349–476.

Albertini, G., Lebihain, M., Hild, F., Ponson, L., Kammer, D.S., 2020. Effective toughness of periodic heterogeneous materials: The role of rate-dependent fracture energy. (under review) .

Amestoy, M., Leblond, J.B., 1992. Crack paths in plane situations - ii. detailed form of the expansion of the stress intensity factors. Int. J. Solids Struc. 29, 465–501.

Auvray, N., Negi, N., Trancart, S., Ponson, L., 2019. L'analyse statistique des faciès de rupture: la science de la donnée au service de l'analyse de défaillance. Traitements & Matériaux 459, 47–50.

Barak, Y., Srivastava, A., Osovski, S., 2019. Correlating fracture toughness and fracture surface roughness via correlation length. Int. J. Frac. 219, 19–30.

Ben-Dayan, I., Bouchbinder, E., Procaccia, I., 2006. Random and correlated roughening in slow fracture by damage nucleation. Phys. Rev. E 74, 146102.

Boffa, J.M., Allain, C., Hulin, J.P., 1998. Experimental analysis of fracture rugosity in granular and compact rocks. Eur. Phys. J. Appl. Phys. 2, 281–289.

Bonamy, D., Bouchaud, E., 2011. Failure of heterogeneous materials: a dynamic phase transition? Phys. Rep. 498, 1–44.

Bonamy, D., Ponson, L., Prades, S., Bouchaud, E., Guillot, C., 2006. Scaling exponents for fracture surfaces in homogeneous glass and glassy ceramics. Phys. Rev. Lett. 97, 135504.

Bouchaud, E., Lapasset, G., Planès, J., 1990. Fractal dimension of fractured surfaces: A universal value? Europhys. Lett. 13, 73–79.

Bouchbinder, E., Mathiesen, J., Procaccia, I., 2004. Roughening of fracture surfaces: The role of plastic deformation. Phys. Rev. Lett. 92, 245505.

Bouchbinder, E., Procaccia, I., Santucci, S., Vanel, L., 2006. Fracture surfaces as multiscaling graphs. Phys. Rev. Lett. 96, 055509.

Cambonie, T., Bares, J., Hattali, M.L., Bonamy, D., Lazarus, V., Auradou, H., 2015. Effect of the porosity on the fracture surface roughness of sintered materials: From anisotropic to isotropic self-affine scaling. Phys. Rev. E 91, 012406.

Chambolle, A., Francfort, G.A., Marigo, J.J., 2009. When and how do cracks propagate. J. Mech. Phys. Solids 57, 1614–1622.

Cotterell, B., Rice, J.R., 1980. Slightly curved or kinked cracks. Int. J. Frac. 16, 155–169.

Crouch, S., 1967. Solution of plane elasticity problems by the displacement discontinuity method. Int. J. Numerical Methods in Engineering 10, 301–343.

Crouch, S., Starfield, A., 1983. Boundary Element Methods In Solid Mechanics. Georges Allen and Unwin.

Dalmas, D., Lelarge, A., Vandembroucq, D., 2008. Crack propagation through phase-separated glasses: Effect of the characteristic size of disorder. Phys. Rev. Lett. 101, 255501.

Demery, V., Rosso, A., Ponson, L., 2014. From microstructural features to effective toughness in disordered brittle solids. EPL 105 34003.

Engøy, T., Måløy, K.J., Hansen, A., Roux, S., 1994. Roughness of two-dimensional cracks in wood. Phys. Rev. Lett. 73, 834–837.

Erdogan, F., Sih, G., 1963. On the crack extension in plates under plane loading and transverse shear. J. Basic Eng 85, 519–525.

Faber, K.T., Evans, A.G., 1983. Crack deflection processes - i. theory. Acta Metall. 31, 565–576.

Gol'dstein, R.V., Salganik, R.L., 1974. Brittle fracture of solids with arbitrary cracks. Int. J. Frac. 10, 507–523.

Hakim, V., Karma, A., 2009. Laws of crack motion and phase-field models of fracture. J. Mech. Phys. Solids 57, 342–368.

Hansen, A., Hinrichsen, E., Roux, S., 1991. Roughness of crack interfaces. Phys. Rev. Lett. 66, 2476–2479.

Hansen, A., Schmittbuhl, J., 2003. Origin of the universal roughness exponent of brittle fracture surfaces: stress weighted percolation in the damage zone. Phys. Rev. Lett. 90, 45504.

Hussain, M.A., Pu, S.L., Underwood, J., 1974. Strain energy release rate for a crack under combined mode i and mode ii , 2–28.

Katzav, E., Adda-Bedia, M., 2013. Stability and roughness of tensile cracks in disordered materials. Phys. Rev. E , 052402.

Katzav, E., Adda-Bedia, M., Derrida, B., 2007. Fracture surfaces of heterogeneous materials: A 2d solvable model. Eur. Phys. Lett. , 46006.

Kertesz, J., Horvath, V., Weber, F., 1993. Self-affine rupture lines in paper sheet. Fractals 1, 67–74.

Lebihain, M., 2019. Large-scale crack propagation in heterogeneous materials : an insight into the homogenization of brittle fracture properties. Ph.D. thesis. Sorbonne Université.

Lebihain, M., Leblond, J., Ponson, L., 2020. Effective toughness of periodic heterogeneous materials: the effect of out-of-plane excursions of cracks. Journal of the Mechanics and Physics of Solids 137.

Mallick, M., Cortet, P.P., Santucci, S., Roux, S.G., Vanel, L., 2007. Discrepancy between subcritical and fast rupture roughness: a cumulant analysis. Phys. Rev. Lett. 98, 255502.

Måløy, K.J., Hansen, A., Hinrichsen, E.L., Roux, S., 1992. Experimental measurements of the roughness of brittle cracks. Phys. Rev. Lett. 68, 213–215.

Mandelbrot, B.B., Passoja, D.E., Paullay, A.J., 1984. Fractal character of fracture surfaces of metals. Nature 308, 721–722.

Melin, S., 1985. The infinitesimal kink. Report LUTFD2/(TFHF-3022)/1-19, Division of solid Mechanics, Lund Institute of Tchnology .

Meng, C., Maerten, F., Pollard, D.D., 2013. Modeling mixed-mode fracture propagation in isotropic elastic three dimensional solid. Int. J. Frac. 179, 45–57.

Millman, V.Y., Stelmashenko, N.A., Blumenfeld, R., 1994. Fracture surfaces: a critical review of fractal studies and a novel morphological analysis of scanning tunneling microscopy measurements. Prog. Mat. Sci. 38, 425–474.

Morel, S., Bonamy, D., Ponson, L., Bouchaud, E., 2008. Transient damage spreading and anomalous scaling in moratr crack surfaces. Phys. Rev. E 78, 016112.

Morel, S., Lubet, T., Pouchou, J.L., Olive, J.M., 2004. Roughness analysis of the cracked surfaces of a face centered cubic alloy. Phys. Rev. Lett. 93, 065504.

Ortiz, J.E., Cisilino, A.P., 2005. Boundary element method for j-integral and stress intensity factor computations in three-dimensional interface cracks. Int. J. Frac. 133, 197–222.

Osovski, S., Srivastava, A., Ponson, L., Bouchaud, E., Tvergaard, V., Ravi-Chandar, K., Needleman, A., 2015. The effect of loading rate on ductile fracture toughness and fracture surface roughness. J. Mech. Phys. Solids 76, 20–46.

Patinet, S., Vandembroucq, D., Roux, S., 2013. Quantitative prediction of effective toughness at random heterogeneous interfaces. Phys. Rev. Lett. 110 165507.

Ponson, L., 2007. Crack propagation in disordered materials: How to decipher fracture surfaces. Ann. Phys. 32, 1–128.

Ponson, L., 2016. Statistical aspects in crack growth phenomena: How the fluctuations reveal

the failure mechanisms. Int. J. Frac. 201, 11–27.

Ponson, L., Auradou, H., Vié, P., Hulin, J.P., 2006a. Low self-affine exponents of fractured glass ceramics surfaces. Phys. Rev. Lett. 97, 125501.

Ponson, L., Bonamy, D., Bouchaud, E., 2006b. Two-dimensional scaling properties of experimental fracture surfaces. Phys. Rev. Lett. 96, 035506.

Ponson, L., Shabir, Z., Abdulmajid, M., der Giessen, E.V., Simone, A., 2021. A unified scenario for the morphology of crack paths in two-dimensional disordered solids. Phys. Rev. E (under review).

Ramanathan, S., Ertas, D., Fisher, D.S., 1997. Quasistatic crack propagation in heterogeneous media. Phys. Rev. Lett. 79, 873–876.

Ramos, O., Cortet, P.P., Ciliberto, S., Vanel, L., 2013. Experimental study of the effect of disorder on subcritical crack growth dynamics. Phys. Rev. Lett. 110, 165506.

Salminen, L.I., Alava, M., Niskanen, K.J., 2003. Analysis of long crack lines in paper webs. Eur. Phys. J. B 2003, 369–374.

Schwaab, M.E., Biben, T., Santucci, S., Gravouil, A., Vanel, L., 2018. Interacting cracks obey a multiscale attractive to repulsive transition. Phys. Rev. Lett. 120, 255501.

Shen, B., Stephansson, O., 1994. Modification of the g-criterion for crack propagation subjected to compression. Engineering fracture mechanics 47, 117–189.

Silva, G.D., Einstein, H.H., 2013. Modeling of crack initiation, propagation and coalescence in rocks. Int. J. Frac. 182, 167–186.

Srivastava, A., Ponson, L., Osovski, S., Bouchaud, E., Tvergaard, V., Needleman, A., 2014. Effect of inclusion density on ductile fracture toughness and roughness. J. Mech. Phys. Solids 63, 62–79.

Vernède, S., Ponson, L., 2015. Method for characterizing the cracking mechanism of a material from the fracture surface thereof , patent WO050871.

Vernède, S., Ponson, L., Bouchaud, J., 2015. Turbulent fracture surfaces: A footprint of damage percolation? Phys. Rev. Lett. 114, 215501.

Wang, N., Xia, S., 2017. Cohesive fracture of elastically heterogeneous materials: An integrative modeling and experimental study. J. Mech. Phys. Solids 98, 87–105.

Williams, M.L., 1952. Stress singularity resulting from various boundary conditions in angular corners of plates in extension. J. Appl. Mech. 19, 526–528.

Zapperi, S., Nukala, P.K., Simunovic, S., 2005. Crack roughness and avalanche precursors in the random fuse model. Phys. Rev. E 71, 026106.